Author Contributions:
Conceptualization: A. Barbeta, D. G. Miralles, J. Carnicer
Data curation: A. Barbeta, L. Mendiola
Formal analysis: A. Barbeta, D. G. Miralles, L. Mendiola, T. E. Gimeno
Funding acquisition: A. Barbeta, D. G. Miralles, J. Carnicer

Disentangling the Role of Forest Structure and Functional Traits in the Thermal Balance of the Mediterranean–Temperate Ecotone

A. Barbeta[1] ⓘ, D. G. Miralles[2] ⓘ, L. Mendiola[3,4], T. E. Gimeno[3,5], S. Sabaté[1,5], and J. Carnicer[1,5]

[1]BEECA-UB, Department of Evolutionary Biology, Ecology and Environmental Sciences, University of Barcelona, Barcelona, Spain, [2]Hydro-Climate Extremes Lab (H-CEL), Ghent University, Ghent, Belgium, [3]Basque Centre for Climate Change (BC3), Leioa, Spain, [4]Errez Kooperatiba Elkarte Txikia, Aramaio, Spain, [5]CREAF, Catalonia, Spain

Abstract The thermal balance of forests is the result of complex land–atmosphere interactions. Different climate regimes and plant functional types can have contrasting energy budgets, but little is known about the influence of forest structure and functional traits. Here, we combined spaceborne measurements of surface temperature from ECOSTRESS with ground-based meteorological data to estimate the thermal balance at the surface ($\Delta T_{can-air}$) during four summers (2018–2021), at the Mediterranean–temperate ecotone in the NE Iberian Peninsula. We analyzed the spatiotemporal drivers of $\Delta T_{can-air}$ by quantifying the effects of meteorology, forest structure (stand density, tree height) and ecophysiology (hydraulic traits), during normal days and hot spells. Canopy temperatures (T_{can}) fluctuated according to changes in air temperature (T_{air}) but were on average 4.2 K warmer. During hot spells, $\Delta T_{can-air}$ was smaller than during normal periods. We attribute this decrease to the advection of hot and dry air masses from the Saharan region resulting in a sudden increase in T_{air} relative to T_{can}. Vapor pressure deficit (VPD) was negatively correlated with $\Delta T_{can-air}$, since the highest VPD values coincided with peaks in heat advection. Nonetheless, T_{can} increased with VPD due to decreased transpiration (following stomatal closure), even though sufficient soil water availability enabled some degree of evaporative cooling. Our findings demonstrate that plot-scale forest structural and hydraulic traits are key determinants for the forest thermal balance. The integration of functional traits and forest structure over relevant spatial scales would improve our ability to understand and model land–atmosphere feedbacks in forested regions.

Plain Language Summary Forests exchange energy with the atmosphere. Different types of forests may result in substantially different energy exchanges, but it is not clear which are the ecological factors causing these differences. This is relevant because during hot spells, the way by which the surface dissipates heat can either intensify or mitigate the air temperature increase. Here, we assessed how canopies exchange heat with the atmosphere depending on the characteristics of the forest cover, in a region densely covered by forests, with great ecological and climatic diversity, in the transition zone between the Mediterranean and the temperate ecotone. We show that recent hot spells were not aggravated by tree energy dissipation into the atmosphere. Instead, we argue that incoming hot air masses, often traveling from northern Africa, reduced the exchange of energy between the surface and the atmosphere, and so, the warming from below was not critical for the aggravation of these hot spells. Yet, we found that there was high variability in the thermal balance of forests along the ecoclimatic gradients of the study region that could not be explained by broad forest type classifications. Instead, differences in the thermal balance and its influence on air temperature were better explained by forests functional and structural characteristics, such as tree height or functional type of the dominant species.

1. Introduction

Biological and physical properties of the Earth's surface regulate the exchange of energy and matter with the atmosphere, by determining the rates and magnitudes of the surface water and energy fluxes (Pitman, 2003). Processes such as evaporation, turbulent sensible heat transfer or the upwelling of shortwave and longwave radiation modulate the local, regional and global climate, and strongly vary as a function of the characteristics of the land cover (Bagley et al., 2017; de Oliveira et al., 2019; Yan et al., 2014). The effects of surface structure on land–atmosphere exchanges, and in turn on local climate, are often well understood; for example, the surface

Investigation: A. Barbeta, L. Mendiola, T. E. Gimeno
Methodology: A. Barbeta, D. G. Miralles, S. Sabaté, J. Carnicer
Project Administration: A. Barbeta, J. Carnicer
Resources: A. Barbeta, L. Mendiola
Software: A. Barbeta
Supervision: A. Barbeta, D. G. Miralles, T. E. Gimeno, S. Sabaté, J. Carnicer
Validation: A. Barbeta, D. G. Miralles, T. E. Gimeno, S. Sabaté, J. Carnicer
Visualization: A. Barbeta, L. Mendiola, T. E. Gimeno, S. Sabaté, J. Carnicer
Writing – original draft: A. Barbeta
Writing – review & editing: A. Barbeta, D. G. Miralles, L. Mendiola, T. E. Gimeno, S. Sabaté, J. Carnicer

properties of cities contribute to the development of urban heat islands, which can be mitigated by increasing vegetation cover (Shiflett et al., 2017). Yet, land surface influences exceed local scales, modulating for instance downwind precipitation patterns (Drumond et al., 2014; Keune & Miralles, 2019; O'Connor et al., 2021; te Wierik et al., 2021). At the regional scale, the onset of extreme temperature episodes is also influenced by a combination of atmospheric dynamics and land–atmosphere feedbacks. There is evidence of direct causal associations between the anomalous heat accumulation in the atmosphere and the preceding low soil moisture, which limits the magnitude of latent heat fluxes over hundreds of square kilometers (Fischer et al., 2007; Miralles et al., 2014, 2019). In addition to the short-term coupling dynamics between land and atmosphere, the impacts of this coupling can reflect over longer timescales (Koster et al., 2004). In fact, changes in land surface biological and physical properties occurring over decadal to centurial scales may have long-lasting global impacts. For instance, the Earth's greening caused by the fertilization effect of anthropogenic CO_2 (e.g., Zhu et al., 2016) may have partially mitigated global warming in recent decades through an increase in evaporative cooling (Forzieri et al., 2017). The interest on the topic of land influence on climate has grown steadily in recent years because of its important implications for future climate (Canadell et al., 2021; IPCC, 2021, p. 20; Seneviratne et al., 2021).

Land vegetation affects land–atmosphere energy, momentum and mass exchanges (Anderegg et al., 2019; Ellison et al., 2017). The characteristics of vegetation regulate how much solar radiation is reflected (Cescatti et al., 2012), partitioned into latent and sensible heat fluxes (Williams & Torn, 2015) or absorbed and temporally stored, thus yielding an increase in surface temperature (Meier et al., 2019). The sole categorization of vegetation into plant functional types (PFTs)—such as conifer/broadleaf forests or grasslands—can help explain changes in surface energy partitioning due to intrinsic properties of these PFTs (Forzieri et al., 2020), such as their leaf area index, which are associated with different ecosystem functions (Migliavacca et al., 2021; Nemani et al., 1996). Besides structural traits, plant physiological traits can also influence the energy balance at the ecosystem-level. For instance, recent studies found that land–atmosphere feedbacks during drought are modulated by plant hydraulic traits and forest specific composition (Anderegg et al., 2018, 2019). This is because evaporative response of forests will depend not only on atmospheric conditions but also on the form and function of specific tree species, and the soil and landscape features that determine access to water resources (Barbeta & Peñuelas, 2017). In another example, Teuling et al. (2010) demonstrated contrasting temporal dynamics of surface energy fluxes during heatwaves in grasslands, which depict a more opportunistic water-use strategy, compared to forests, with a more conservative water use. Grasslands respond to heat with a fast increase in transpiration that initially minimizes sensible heat fluxes, but as soil moisture is depleted, sensible heat fluxes progressively increase. In contrast, the more conservative water-use in forests, combined with their lower albedo, yields an initially stronger increase in sensible heat fluxes; after a few days, however, forests prevent heatwave amplification due to the sustained transpiration enabled by a usually deeper root system. This example shows that differences among plant functional types are critical to understand how the land feeds back into the atmospheric state, and particularly during the evolution of hot spells. A key trait driving the energy balance of the vegetation is surface conductance, defined as the inverse of the resistance to water diffusion along the soil–plant–atmosphere continuum (Wang et al., 2019). To date, the study of the biotic determinants of surface conductance has been, typically restricted to the consideration of different PFTs (Gerken et al., 2019; Teuling et al., 2010). However, there is evidence that the surface conductance can drastically differ among different types of forest and plant species (Wang et al., 2019).

Canopy temperature (T_{can}) is largely driven by incoming radiation, and it determines sensible heat, water and carbon fluxes (Still et al., 2021). Deviations of T_{can} from air temperature (T_{air}) are often associated with fluctuations in surface and aerodynamic resistance to the heat transfer by conduction and convection (sensible heat flux) (Grace, 1988). Simultaneously, T_{can} influences and is influenced by tree transpiration, which reduces the temperature of the leaves by 'evaporative cooling' (Javadian et al., 2022). The difference between T_{can} and T_{air} (i.e., $\Delta T_{can-air}$) can be seen as the integrative result of all the components of the energy balance of the canopy. From the biological point of view, the relationship between T_{can} and T_{air} can be an indicator of plant water stress (Fauset et al., 2018; Moyano et al., 2018). From an atmospheric standpoint, $\Delta T_{can-air}$ may reflect the influence of non-local controls on T_{air} (e.g., advection, entrainment, subsidence, condensation). As such, estimating $\Delta T_{can-air}$ at high temporal and spatial resolutions provides valuable insights into dynamic land–atmosphere feedbacks and how these are modulated by plant water-use strategies (Anderegg et al., 2019; Wang et al., 2019). This approach can help elucidate how biotic and abiotic determinants interact and affect the surface energy balance of forests.

In recent years, there has been an increase in the spatial and temporal resolution of remote sensing products measuring land surface temperature (LST) that may be used as a proxy for T_{can} in vegetated regions. More specifically,

the ECOsystem Spaceborne Thermal Radiometer Experiment on Space Station (ECOSTRESS) launched in 2018 by the National Aeronautics and Space Administration (NASA) provides LST at a spatial resolution of 70×70 m, every 3–5 days (Fisher et al., 2020) and with high accuracy (Hulley et al., 2022). Interestingly, this high spatial resolution enables the coupling of remotely sensed LST with plot-scale variations in forest structure, environmental conditions or any other variable measured at the fine scale (Javadian et al., 2022). It is thus possible to achieve more detailed, mechanistic-oriented analyses of the forest thermal balance, beyond the comparison of the thermal balance between different vegetation types.

Here we leverage the availability of spatially dense data sets on forest structure, meteorological conditions and topography for an ecologically and climatically diverse area in the Mediterranean–temperate ecotone to investigate $\Delta T_{can-air}$, and its drivers over the growing season. Particularly, we hypothesize that (a) $\Delta T_{can-air}$ will be higher during hot spells than in normal days due to reduced transpiration and evaporative cooling and that (b) forests with a more conservative water-use and occupying the warmer and drier areas will present a relatively higher $\Delta T_{can-air}$ during hot spells due to reduced transpiration rates (see e.g., Teuling et al. (2010)). Low water availability should be correlated with forest structural properties—such as lower LAI, aboveground biomass and basal area—so we do not expect structural variables to explain additional variability in $\Delta T_{can-air}$, beyond that explained by climatic gradients (mean precipitation, temperature and radiation). On the other hand, we also hypothesize (c) a strong effect on $\Delta T_{can-air}$ of variables that are directly related to heat dissipation through their effect on surface roughness (Muller et al., 2021). Specifically, we expect that larger canopy height, canopy cover and stand density (all variables analyzed here) have independent (and negative) effects on $\Delta T_{can-air}$. Finally, since low transpiration rates should lead to higher $\Delta T_{can-air}$, we also hypothesize that (iv) forests dominated by drought-resistant species (with a certain suite of associated hydraulic traits) would show higher $\Delta T_{can-air}$, compared to those dominated by more drought-sensitive species (Still et al., 2022). However, it would also be possible that some drought-sensitive species with access to deep-water could maintain relatively high transpiration rates during hot spells (Krich et al., 2022), and hence lower $\Delta T_{can-air}$.

2. Data and Methods

2.1. Study Area

The selected study area corresponds to Catalonia, an area covering 32,114 km^2 in the NE of the Iberian Peninsula, in the NW shores of the Mediterranean Sea. Catalonia is located at the transition zone between Mediterranean and temperate climates, so its climate is predominantly Mediterranean, but is also subjected to Atlantic, temperate and subtropical influences (Llebot, 2005). The complex orography in this area results into a high diversity in thermic regimes across an altitude range from sea level to >3,000 m a.s.l., as well as into drier/wetter areas due to leeward/ windward exposures relative to the Mediterranean sea, but also to the Atlantic Ocean (Martín Vide, 2016). Hence, Catalonia depicts an unusually high climatic diversity for such a small area, which ranges from cold semi-arid climates (BSk in the Köppen–Geiger classification) to temperate ones (e.g., Cfa or Cfb in the same classification system), with coastal areas presenting a typical hot-summer Mediterranean climate (Csa) (Beck et al., 2018). As such, mean annual precipitation (MAP) ranges widely, from 350 to 1,300 mm, with mean annual temperatures (MAT) ranging from 0 to 17°C (Llebot, 2005). In line with the climatic diversity of the area, the relatively high fraction of forested area—ca. 38% (Rosas et al., 2019)—is occupied by functionally and structurally diverse forests, mostly dominated by tree species from the Fagaceae and Pinaceae families (Roces-Díaz et al., 2018). The lowland forests in the coastal areas are dominated by broadleaf evergreen tree species, such as *Quercus ilex* L., and needleleaf Mediterranean trees, such as *Pinus halepensis* Mill., the latter occupying the drier coastal area and the inland lowland areas (Figure 1). Moister and cooler areas at mid altitudes (500–1,600 m), and often with a maritime influence, harbor forests dominated by broadleaf deciduous species, some common across Europe (e.g., *Fagus sylvatica* L., *Fraxinus excelsior* L.), but also trees typical of the Mediterranean–temperate biome transition (e.g., *Quercus pubescens* Willd., *Quercus faginea* Lam.). In the mid to high altitudes of the Pyrenees, we find needleleaf montane forests dominated by coniferous species that reach their southernmost distribution range in the study area, such as *Abies alba* Mill., *Pinus uncinata* Ram. and *Pinus sylvestris* L. (Figure 1). The diversity in forest structure, function and environmental conditions makes the area especially suitable for our research goals.

2.2. Forest Structural, Topographical and Meteorological Data and Species-Specific Hydraulic Traits

The data set comprises 4,131 forest plots belonging to the Fourth Spanish Forest National Inventory (IFN4) conducted between 2013 and 2016 (https://www.miteco.gob.es/es/biodiversidad/temas/inventarios-nacionales/
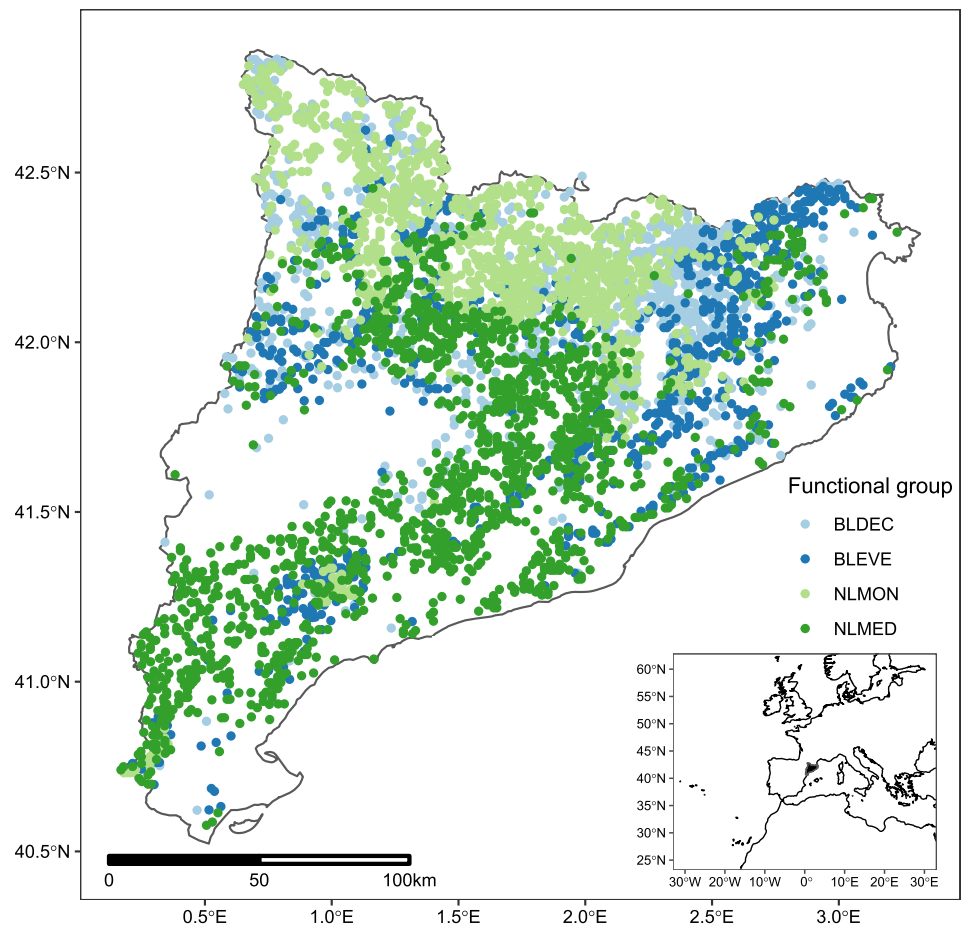
Figure 1. *Study area*. Map of Catalonia and the forest plots included in the analysis, with colored dots illustrating the functional group of the dominant species of each plot (light blue: BLDEC, broadleaf deciduous, dark blue: BLEVE, broadleaf evergreen, light green: NLMON, needleleaf montane, dark green: NLMED, needleleaf Mediterranean). Inset: the black area represents the location of the study area (Catalonia) within the Western Mediterranean Basin.

inventario-forestal-nacional/cuarto_inventario.aspx). From this inventory, we extracted data on forest stand composition, that is, the dominant species, according to measurements of basal area and the percentage of basal area of the dominant species. A forest with more than 80% of basal area of the same species was considered a pure stand; conversely, those stands in which the basal area of the dominant species was below 80% were considered as mixed. From the IFN4, we also extracted plot topographic information including the elevation, the aspect of the plot (North, South, East, West or flat), the slope of the terrain (%) and the type of curvature, where positive values denote a concave curvature (i.e., hills) and negative values denote a convex curvature (i.e., valleys). Average climatic data for each plot was also available (see Table S1 in Supporting Information S1). Forest structural data was extracted from each of the IFN4 plots from a LIDAR-based data set with a 20×20 m resolution collected between 2008 and 2011 and processed by the Center of Ecological Research and Forest Applications (CREAF) and the Catalan Geologic and Cartographic Institute (ICGC). The variables included in our analysis were: total aerial biomass, foliar biomass, basal area, tree cover, diameter at breast height (DBH), leaf area index, stand density and mean tree height (Table S2 in Supporting Information S1). In addition, we used a data set on tree hydraulics traits collected in the same forest plot network across aridity gradients of the six most abundant species; a detailed description of the methods used to measure the hydraulic traits is provided by Rosas et al. (2019). Because of the large number of dominant species represented in our data set (60, according to our dominance criteria based on basal area, Barbeta et al., 2022), for some of our analyses we grouped species in four functional groups: needleleaf Mediterranean (NLMED), needleleaf montane (NLMON), broadleaf evergreen (BLEVE) and broadleaf deciduous (BLDEC).

Meteorological data specific for the location of each plot and for the period 2018–2021 was obtained using the R package *meteoland* (De Cáceres et al., 2018). This package provides estimates of daily weather variables over

the landscape by spatial interpolation of daily weather records, at a resolution of 30×30 m, and accounting for the effects of elevation, slope, and aspect. For the present data set, data from stations of the Spanish State Meteorology Agency (AEMET) and the Catalan Meteorological Service (SMC) were used as input data. The meteorological data included daily air temperature, relative humidity, wind speed, precipitation, potential evaporation and solar radiation. With the interpolated variables we also calculated the climatic water balance (CWB) of the 30 days prior to the remote sensing measurement (precipitation minus potential evaporation), for each plot. After the spatial interpolation using *meteoland* (De Cáceres et al., 2018), midday daily vapor pressure deficit (VPD) was estimated with the *rh.to.VPD* function from the R package *bigleaf* (Knauer et al., 2018). Next, we downscaled these interpolated daily data on wind speed, air temperature (T_{air}, at canopy height) and relative humidity to hourly scales, using hourly data from the network of automatic meteorological stations XEMA (https://www.meteo.cat/observacions/xema), so that each meteorological observation would be more comparable to the overpass of ECOSTRESS. Air temperature at ground-level was transformed into air temperature at canopy height, by using temperature scales in forested surfaces (Bonan, 2015)—see Text S1 in Supporting Information S1 for further details.

Forest structural, topographical and meteorological data were accessed through the R package *lfcdata* (https://github.com/MalditoBarbudo/lfcdata), which gives direct access to the data of the Catalan Forest Laboratory (https://laboratoriforestal.creaf.cat/), an initiative of CREAF and the Forest Science and Technology Center of Catalonia (CTFC). We also obtained shortwave albedo data from MODIS MCD43A3 data sets that provide both black-sky and white-sky albedo. We used only black-sky albedo (directional hemispherical reflectance) for the analysis, yet these values were highly correlated with white-sky albedo ($R^2 = 0.96$). We calculated the average black-sky albedo from June to September for each of the plots and the period of study.

2.3. Land Surface Temperature (LST) Data From ECOSTRESS

We retrieved LST data from the ECOsystem Spaceborne Thermal Radiometer Experiment on Space Station (ECOSTRESS, https://ecostress.jpl.nasa.gov/), particularly, from the ECO2LSTE Version 1, a Level-2 product from ECOTRESS. ECO2LSTE provides LST at a spatial resolution of 70×70 m and every 3–5 days (Fisher et al., 2020). Our choice of ECOSTRESS over other remotely sensed LST products was based on the unique combination of high spatial resolution and relatively more frequent observations. For each of the forest plots in our network, we downloaded the LST for all dates available in the ECO2LSTE Version 1 collection through the Application for Extracting and Exploring Analysis Ready Samples (AρρEEARS) data portal. From that, we used the product quality flags to select only those clear sky observations with the best quality and a LST accuracy below 1.5 K. The period spanned from the beginning of the ECOSTRESS mission (2018) to December 2021. Here, we only used data from June–September, comprising the growing season in the study area. Finally, we selected only observations corresponding to the central hours of the day (9–15 hr UTC), during which the vegetation transpires and thus dynamically influences LST.

2.4. Data Processing

Daily meteorological data for each plot (wind speed, air temperature at canopy height and relative humidity) were obtained by spatial interpolation (De Cáceres et al., 2018) (see Section 2.3 for further details) and maximum daily vapor pressure deficit (VPD) was estimated with the *rh.to.VPD* function from the R package *bigleaf* (Knauer et al., 2018). Next, we downscaled these interpolated daily data on wind speed, air temperature (T_{air}, at canopy height) and relative humidity to hourly scales, using hourly data from the network of automatic meteorological stations XEMA (https://www.meteo.cat/observacions/xema), so that each meteorological observation would be more comparable to the overpass of ECOSTRESS. Once we had a complete database of air temperature (T_{air}) collocated with their corresponding LST observation (T_{can}, from the ECO2LSTE version 1 (see Section 2.3), we calculated $\Delta T_{can-air}$, that is, the difference (between land (T_{can}) and air temperature (T_{air}). Positive values of $\Delta T_{can-air}$ indicate that the land surface (i.e., the forest upper canopy) is warmer than the free air above it, whereas negative values indicate that the land surface is cooler.

Our study period (June–September 2018–2021) was divided into normal periods and hot spells. According to the Catalan Meteorological Service, hot spells are defined as periods in which temperatures above the 98th percentile of June–August maximum temperatures (according to a 10-year record) at any given *XEMA* meteorological

station. Hot spells are considered a heatwave when they last for 3 days or more. During the 2018–2021 study period, the area experienced five hot spells.

2.5. Statistical Analysis

We first tested for the effect of several categorical variables on $\Delta T_{can-air}$ and T_{can}: (a) functional group of the plot's dominant species, (b) stand composition (pure vs. mixed stands). We also assed (c) differences between normal and hot spell days. For each of these fixed categorical factors we fitted a generalized linear mixed model (GLMM) with hour of the observation, aspect of the plot and the plot identifier as random factors, using the function *lmer* of the R package *lme4* (Bates et al., 2015). The mean annual precipitation was also added to these models to account for gradients in annual rainfall. We then checked for pairwise differences with Tukey post-hoc tests from the R package *emmeans* (Lenth et al., 2018). Next, we tested for the effects of continuous forest variables on $\Delta T_{can-air}$ and T_{can}. We initially considered the correlation with 19 variables characterizing forest structure (basal area, stand density, tree cover, total aerial biomass, DBH, mean tree height, foliar biomass, LAI, and albedo), topography (slope, curvature and distance to the sea), meteorology (30-day climatic water balance, VPD, solar radiation and wind speed) and climate (mean annual temperature (MAT), mean annual precipitation (MAP) and mean daily solar radiation). In order to assess the independent and interactive effects of all these variables on $\Delta T_{can-air}$ and to quantify their relative importance, we followed the recommendations of Murray and Conner (2009). In brief, we first computed zeroth-order correlations and eliminated those variables that presented near-zero correlations with $\Delta T_{can-air}$. In a second step, we ran hierarchical partitioning of the variance for each family of variables (forest structure, topographical, climatic and meteorological) to rank the importance of these variables and discard those with small independent contributions (Mac Nally & Walsh, 2004). Selected variables were included in a *lmer* mixed model, for which we confirmed the absence of multicollinearity effects using the *performance* R package (Lüdecke et al., 2020). Then, we included in the final model those variables that improved the Akaike Information Criterion (AIC) of the model (Akaike, 1974). Finally, we ran a general mixed model to assess the effects of continuous environmental variables, in which we included functional group and stand composition (pure vs. mixed), hour of the observation, aspect of the plot and the MAP decile as random factors. To compare the relative effects of model variables, we estimated *beta* (standardized) coefficients. We also ran a similar model but with T_{can} as dependent variable, instead of $\Delta T_{can-air}$.

The data on tree functional and hydraulic traits from Rosas et al. (2019) were obtained from the same area and forest plot network as for the rest of data. However, trait data was only available for the six most abundant species in the area, including two needleleaf Mediterranean trees (NLMED; *Pinus halepensis* and *Pinus nigra*), one needleleaf montane tree (NLMON; *Pinus sylvestris*), one broadleaf evergreen tree (*Quercus ilex*) and two broadleaf deciduous trees (*Fagus sylvatica* and *Quercus pubescens*). Rosas et al. (2019) sampled 15 plots of each of these six species, categorized across percentiles of the growing season climatic water balance (from dry to medium to wet according to the <33rd, 33rd–66th and >66th percentiles, respectively) calculated at the species-specific level, for the whole forest plot network. This allowed us to estimate trait averages across species and percentiles of climatic water balance (25 individuals in each combination of species and type of climate). We categorized the climatic water balance of the growing season of all plots classified as pure stands (>80% in basal area) of the six species studied in Rosas et al. (2019), and computed group means (and their corresponding standard errors) of $\Delta T_{can-air}$ and T_{can} for all observations of the study period in normal days and hot spells, separately. We also extracted the β coefficients of the correlation between $\Delta T_{can-air}$ and T_{can} and VPD, for the same groups. We then calculated linear correlations of $\Delta T_{can-air}$, T_{can}, and their correlation with VPD with the following traits: specific leaf area (SLA), xylem pressure at the 50% loss of conductivity (P50), xylem pressure at the turgor loss point (ψ_{tlp}), stem specific conductivity (k_s), leaf specific conductivity (k_l), leaf lifespan, leaf carbon isotopic composition ($\delta^{13}C$), wood density, leaf thickness and Huber value (sapwood to leaf area ratio at the branch level). In a second step, we set the "*species*" as random factor to determine whether inter-specific trait differences could explain any potential correlation. All data processing and statistical analyses were carried out using the software R, version 4.1.2 (R Core Team, 2021).

3. Results

3.1. Thermal Balance of Forests

As estimated by the data collected by ECOSTRESS, T_{can} was on average (±se) 4.18 ± 0.03 K warmer than T_{air}, ranging from −2.17 to 12.2 K (5th and 95th percentiles of $\Delta T_{can-air}$, respectively), for June–September of 2018–
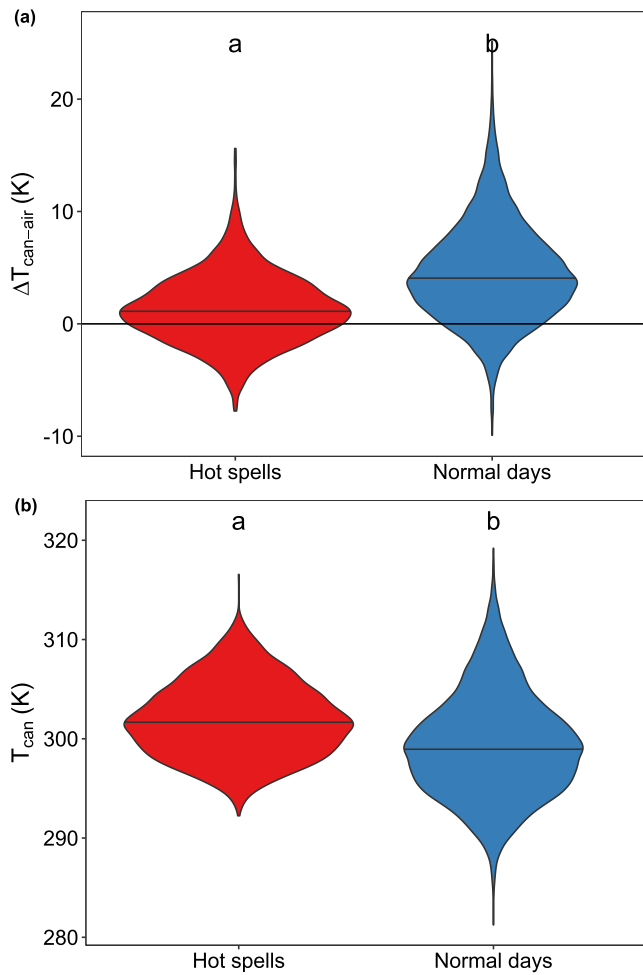
Figure 2. The thermal balance ($\Delta T_{can-air}$) (a) and canopy temperature (T_{can}) (b) in hot spells and normal days. For both $\Delta T_{can-air}$ and T_{can} differences between hot spells and normal days were significant, as noted by the different letters above each group of data points.

2021 and from 9 to 15hr UTC. There was a significant ($p < 0.001$) effect of the hour of the measurement on T_{can}; a peak in $\Delta T_{can-air}$ (8.12 ± 0.13 K) was observed at 13hr UTC coinciding with a peak in T_{can} (303.7 ± 0.15 K) (Figure S1 in Supporting Information S1). In contrast, during hot spells, the higher forest T_{can}, compared to normal days (301.9 ± 0.08 K vs. 299.3 ± 0.03 K, $p < 0.001$) was not accompanied by an also higher $\Delta T_{can-air}$, in fact $\Delta T_{can-air}$, was significantly lower during hot spells (1.32 ± 0.07 K vs. 4.50 ± 0.09 K, $p < 0.001$) (Figure 2). Over the study period, there were significant differences within the growing season among months in both $\Delta T_{can-air}$ and T_{can}. First, observations for the month of July were very scarce (Figure S2 in Supporting Information S1). For the rest of the months, the warmest T_{can} was estimated for August, followed by June, and September (all differences at least $p < 0.01$) (Figure S3 in Supporting Information S1). For $\Delta T_{can-air}$, the largest values were estimated for the months of September, followed by June, and August ($p < 0.01$) (Figure S3 in Supporting Information S1). The species composition of the stand also had significant influence on $\Delta T_{can-air}$. Mixed forests presented lower $\Delta T_{can-air}$ compared to pure forests (3.28 ± 0.05 K vs. 4.53 ± 0.04 K, $p < 0.001$) (Figure S4 in Supporting Information S1). Likewise, the functional group of the dominant species also had a significant effect on the thermal balance of the forest (Figure 3). To test for differences in $\Delta T_{can-air}$, we accounted for the spatial and temporal distribution of the observations using random factors and included the precipitation gradients as a fixed factor. As a result, pairwise comparisons among the four different functional groups revealed significant differences in $\Delta T_{can-air}$ ($p < 0.05$) that were not apparent in raw observations (Figure 3a). The statistical model revealed that NLMED had the lowest $\Delta T_{can-air}$. NLMON and BLDEC had significantly higher $\Delta T_{can-air}$ than NLMED (Figure 3a). BLEVE had the highest $\Delta T_{can-air}$, but not significantly higher than NLMON. On the other hand, T_{can} was significantly different in each group, being warmer in drier plots and following the thermal niche of each group (NLMED > BLEVE > BLDEC > NLMON, Figure 3).

3.2. Drivers of the Spatiotemporal Variability in $\Delta T_{can-air}$ and T_{can}

We considered several plot-level structural, topographical, climatic, and daily meteorological continuous predictors that could affect $\Delta T_{can-air}$ and T_{can}. By means of hierarchical partitioning and generalized linear mixed models (see Section 2.5), we identified 11 variables that explained 15.4% of the variance of $\Delta T_{can-air}$ in the GLMM (40.5% including random effects). The standardized β coefficients showed that the strongest correlation with $\Delta T_{can-air}$ was found for MAT, followed by the effects of MAP, albedo, and VPD (Figure 4a).

According to the mixed model, $\Delta T_{can-air}$ tended to be closer to zero in tall forests (>20 m) with a high density and tree cover fraction, likely due to the higher surface roughness and aerodynamic conductance (Figure S5 in Supporting Information S1). Unsurprisingly, meteorological conditions were more strongly correlated with $\Delta T_{can-air}$ than with T_{can}, due to the direct dependency of T_{air} on atmospheric (thermo)dynamics. $\Delta T_{can-air}$ was closer to zero under high VPD, suggesting a control of warm air advection over T_{air}. The climatic water balance (CWB) of the last 30 days was negatively correlated with $\Delta T_{can-air}$, indicating that wetter conditions were associated with a $\Delta T_{can-air}$ closer to zero, as expected. The correlation with mean annual radiation was small, compared to other climatic variables, but still, more radiation was associated with more positive $\Delta T_{can-air}$. In addition, forests in steeper slopes had low $\Delta T_{can-air}$ compared to those in flatter areas. The correlation of $\Delta T_{can-air}$ with VPD was significantly modified by the CWB (Figure 5a). The negative correlation of $\Delta T_{can-air}$ with VPD was stronger under wet conditions (positive CWB), whereas it tended to vanish under drought due to the increase in T_{can} (Figure 5).

The mixed model for T_{can} explained 71.2% of its variance, with fixed factors (the same that were selected for $\Delta T_{can-air}$) explaining 64.2%. VPD was the factor with the highest correlation, even more than other climatic
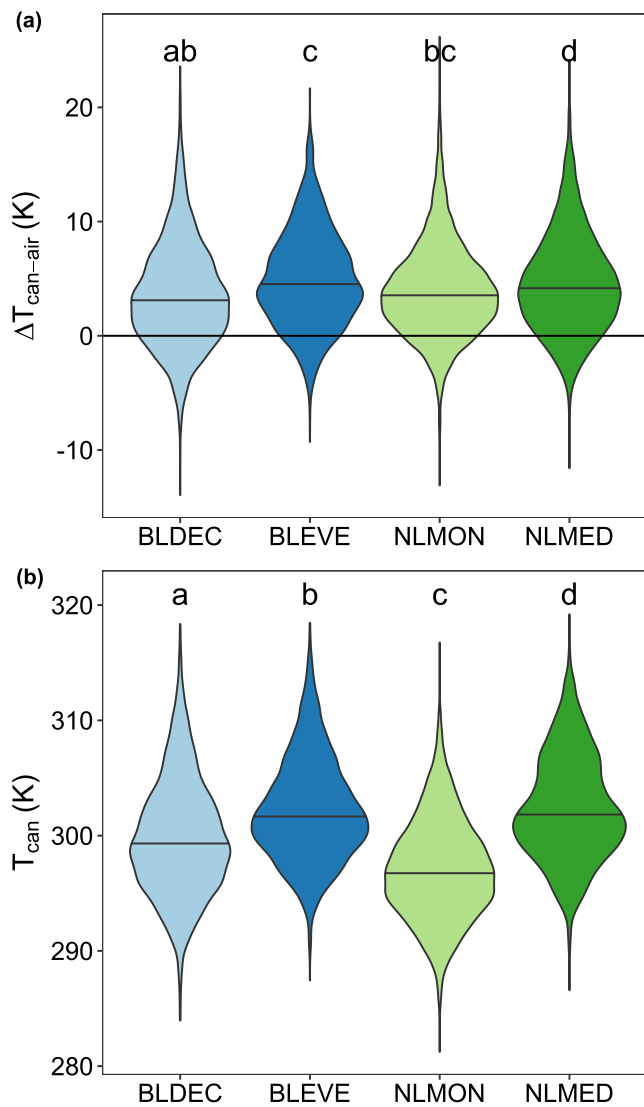
Figure 3. The thermal balance ($\Delta T_{can-air}$) (a) and canopy temperature (T_{can}) (b) across different forest types. Forest types are broadleaf deciduous (BLDEC), broadleaf evergreen (BLEVE), needleleaf montane (NLMON), and needleleaf Mediterranean (NLMED). Letters on top of each group of data points (a, b, c, or d) indicate significant differences between these groups as obtained with the GLMM. Note that statistical differences in $\Delta T_{can-air}$ estimated with GLMM do not coincide with those derived by the medians of the observations of each group, because spatial and temporal factors were included as random factors (see Section 2.5 for details).

variables. Although in this case the correlation with VPD was positive: high VPD was associated with hotter T_{can}. We note that this may occur due to the partial stomatal closure in response to high VPD, or due to the influence of heat advection constraining the ability of the canopy to dissipate heat via sensible heat flux. On the other hand, CWB was associated with cooler T_{can}. The interaction between VPD and CWB was significant for T_{can}. Model predictions show that the positive correlation between VPD and T_{can} shifted to negative in wetter sites (Figure 5b). In general, meteorological variables appeared to be more relevant than forest structural variables for T_{can} (Figure 4b). Still, we observed that cooler T_{can} was associated with tall forests with high tree cover and stand density, whereas higher albedo was associated with hotter T_{can}.

3.3. Effect of Plant Functional Traits on $\Delta T_{can-air}$ and T_{can}

Plant functional traits measured in Rosas et al. (2019) were associated with average $\Delta T_{can-air}$ across water availability gradients of the six most common tree species in the study area. We computed the correlation of plant functional traits with $\Delta T_{can-air}$ and found out that five out of the 10 considered traits presented significant ($p < 0.05$) relationships in normal days (Table S3 in Supporting Information S1). After accounting for inter-specific variability (i.e., with the inclusion of *species* as a random factor in the models) the effect of plant functional traits on $\Delta T_{can-air}$ largely became not significant (Table S4 in Supporting Information S1). Still, $\Delta T_{can-air}$ showed a marginally significant relationship with the xylem pressure at 50% loss of conductivity (P50, Figure 6a); trees with higher resistance to conductivity losses tended to have more positive values of $\Delta T_{can-air}$. We then tested if plant functional traits were associated with the response of $\Delta T_{can-air}$ to VPD. We found positive and significant effects of P50, leaf $\delta^{13}C$, specific leaf area (SLA), and the xylem pressure at turgor loss point (ψ_{tlp}) on the VPD–$\Delta T_{can-air}$ relationship. This means that forests dominated by species with higher water-use efficiency (higher $\delta^{13}C$), resistance to cavitation and turgor loss, and lower SLA also exhibited greater $\Delta T_{can-air}$ increases in response to high VPD, in normal days (Figure 6c). Interestingly, the effect of P50 and leaf $\delta^{13}C$ on VPD–$\Delta T_{can-air}$ was significant but shifted their sign during hot spells (Figure 6d and Tables S3 and S4 in Supporting Information S1).

T_{can} was significantly associated with plant hydraulic traits of the most common species of the study area (see Table S5 in Supporting Information S1 for full results). During both normal periods and hot spells, T_{can} was warmer in forests dominated by species with higher resistance to conductivity losses (P50), more efficient water-use ($\delta^{13}C$) and more negative xylem pressure at the turgor loss point (ψ_{tlp}) (Figures 6e and 6f and Table S5 in Supporting Information S1). Thus, forests dominated by species with a vascular system that is more resistant to water stress tended to exhibit hotter T_{can}. The correlation of VPD with T_{can} was also dependent on leaf $\delta^{13}C$ during hot spells, but also on the leaf-to-sapwood area ratio (Huber value), leaf thickness, and leaf lifespan (Figure 6h, Table S5 in Supporting Information S1). Forests dominated by species with higher resistance to conductivity losses (P50) were the only ones showing a decrease in T_{can} in response to the high VPD experienced during hot spells. In fact, those cases corresponded to the Mediterranean needleleaf *Pinus halepensis*.

4. Discussion

### 4.1. Plot-Scale Measurements of the Canopy Thermal Balance With ECOSTRESS

In this study, we leveraged the availability of high-resolution LST data from ECOSTRESS to estimate the canopy thermal balance (as diagnosed by $\Delta T_{can-air}$) at a spatial scale that allows integration with forest structural data
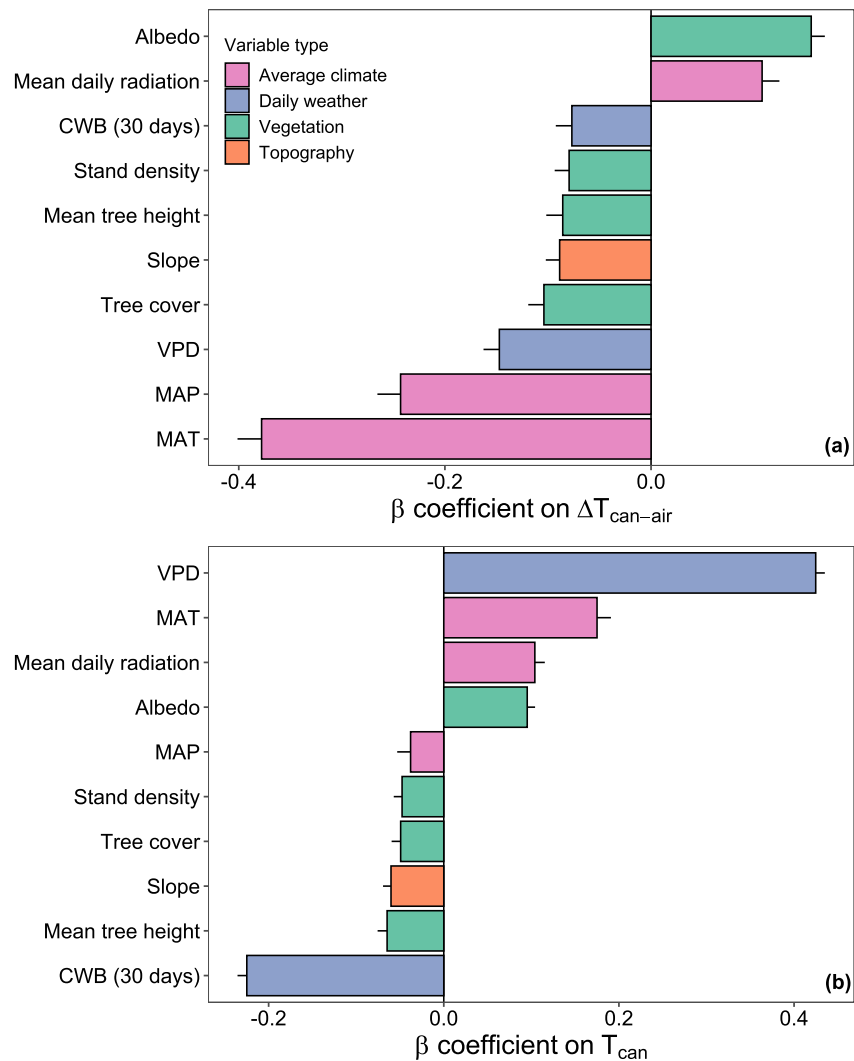
Figure 4. Drivers of the thermal balance ($\Delta T_{can-air}$) and the canopy temperature (T_{can}). Standardized β coefficients of the effect of the average climate (pink), daily weather (blue), forest structural (green) and topographical (orange) variables on $\Delta T_{can-air}$ (a) and T_{can} (b). Positive (negative) coefficients on $\Delta T_{can-air}$ imply correlations with warm (cool) T_{can} relative to T_{air}. Positive (negative) coefficients on T_{can} imply correlations with warmer (cooler) values of T_{can}. All variables included in the mixed model were significant ($p < 0.001$). Uncertainty bars are the standard error of the mean, estimated for each individual effect. Effects are sorted based on their beta coefficient.

from forest inventories and plant functional traits. On average, our estimations of $\Delta T_{can-air}$ were slightly higher than those from montane coniferous forests in both warm and cold seasons, but our range was similar (Javadian et al., 2022). This range was broad, which could be caused by the wide ecoclimatic gradient covered by the study area, including structurally and functionally different forests over a wide range of MAP (from 350 to 1,300 mm, Table S1 in Supporting Information S1). Thus, our study included forests that are drier than those from studies in other temperate areas where $\Delta T_{can-air}$ was estimated to be ca. 1 K lower (Still et al., 2022; Yi et al., 2020). Importantly, the estimated $\Delta T_{can-air}$ derived from ECOSTRESS was comparable to the $\Delta T_{can-air}$ obtained with in situ thermal imaging for high elevation shrublands and meadows (Blonder et al., 2020) and temperate needleleaf and broadleaf forests (Still et al., 2022). While the area covered by infrared cameras is inevitably limited, their observations can be individual-specific. On the contrary, analyses of the relationship between T_{air} and T_{can} from remote sensing usually have a spatial resolution (ca. 0.5°) that exceeds the scale at which forest plot measurements are collected. Our approach takes advantage of the best of these two approaches: the high spatial coverage of satellite observations and the high spatial resolution provided by the novel ECOSTRESS thermal sensor. This allows not only for a better understanding of how heat and water exchange over time and space (Xiao et al., 2021), but also
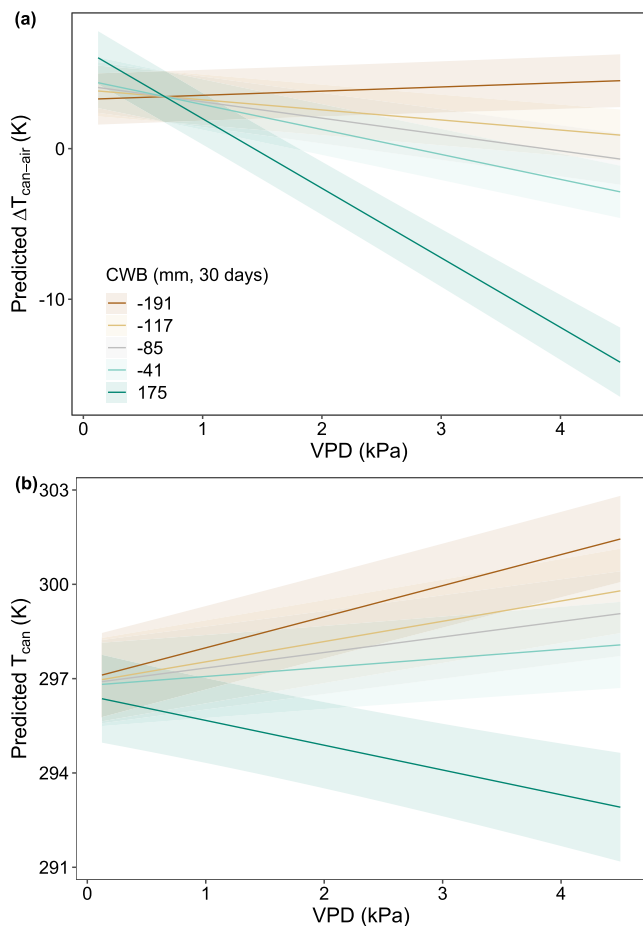
Figure 5. Interactive effects of vapor pressure deficit (VPD) and climatic water balance (CWB) on the thermal balance ($\Delta T_{can-air}$) and the canopy temperature (T_{can}). Model predictions of $\Delta T_{can-air}$ (a) and T_{can} (b) as a function of the VPD and the climatic water balance (CWB) of the previous 30 days. Line colors illustrate different levels of CWB, from drier (negative) to wetter (positive) conditions. The shades around the lines correspond to the 95th confidence intervals of the predicted $\Delta T_{can-air}$. The interaction between VPD and CWB was significant in the mixed models.

enables us to associate these exchanges with fine-scale variations in forest structure and function (Cooley et al., 2022).

4.2. Heat Advection Influence on Forest $\Delta T_{can-air}$ Patterns

During hot spells, $\Delta T_{can-air}$ was significantly lower than in normal days, regardless of the type of forest and its average climate (Figure 2a). Hot spells in the Iberian Peninsula are usually caused by the heat advection associated with Saharan air intrusions (Sousa et al., 2019). The warm and dry air carried by these intrusions results in a lower $\Delta T_{can-air}$ driven by a sudden increase in T_{air}. Hence, during hot spells although T_{can} was still higher than in normal days (Figure 2b), the increase experienced in T_{air} was even larger. As T_{air} increases, canopy-to-air sensible heat fluxes will be inhibited (Still et al., 2021). As a result, the amplification of hot spells by local sensible heat fluxes would be comparably unimportant, and thus the forest canopies would not have a positive feedback on hot spell occurrence. Instead, the studied hot spells would be largely driven by circulation and the advection of heat, rather than accompanied by changes in incoming radiation and subsequent sensible heat fluxes (Figure S6 in Supporting Information S1). Therefore, the response to hot spells of the forest thermal balance in this Mediterranean region seems to contrast with the important influence of soil desiccation found in higher latitudes (Schumacher et al., 2019; Teuling et al., 2010).

While heat advection appears to be a key component of the forest thermal balance, we still found that $\Delta T_{can-air}$ was a function of local climatic gradients and daily meteorological conditions across the studied forest plot network. Spatial variability in rainfall and solar radiation exerted negative and positive effects, respectively, on both $\Delta T_{can-air}$ and T_{can}. This can be expected because solar radiation warms the surface (T_{can}), and the availability of water governs the partitioning of that radiation between sensible and latent heat fluxes. T_{can} was on average warmer in locations with warmer mean annual temperatures (Figure 4b). During hot spells, heat advection results in decreases in $\Delta T_{can-air}$. This explains the negative correlation between VPD and MAT with $\Delta T_{can-air}$ (Figure 4a). High VPD during hot spells coincides in space and time with low $\Delta T_{can-air}$, as opposed to what could be expected if the high VPD was a response to dry and warm surfaces. In summary, increases in T_{air} are externally driven by advection, and not by local sensible heat fluxes because in that case, we should have observed a positive relationship between $\Delta T_{can-air}$ and VPD.

VPD is one of the main drivers of canopy transpiration (Flo et al., 2021; Grossiord et al., 2020), but transpiration responses to high VPD range from strong decreases to strong increases as a function of the plants' water use strategy (Massmann et al., 2019). Initially, in moist temperate forests, moderate increases in VPD may enhance transpiration rates and cool down the canopy (Yi et al., 2020). Yet, in water-limited areas, such as the one studied here, canopy transpiration tends to decline with increases in VPD (Duursma et al., 2014; Flo et al., 2021). This agrees with the positive correlation between high VPD and warm T_{can} that we observed under dry conditions (Figure 5b) showing that high VPD prevents the transpiration-driven cooling of the canopy. Yet, increasing VPD should still result in cooler canopies when water is still available for plants (Figure 5b). Indeed, we found lower $\Delta T_{can-air}$ and cooler T_{can} under wetter conditions (Figure 4), which we attributed to the increase in transpiration when the soil is moist in these water-limited environments. Our results are consistent with observations from tropical regions, where water availability in the upper soil layers strongly controls surface temperature (Green et al., 2022). Similarly, in temperate regions, the deeper root systems of forests compared to grasslands also result in more transpirational cooling and lower temperatures (Lansu et al., 2020; Teuling et al., 2010; Zhang et al., 2020), emphasizing the importance of root water uptake for predicting vegetation-atmosphere feedbacks (Barbeta & Peñuelas, 2017; Cabon et al., 2018). Access to deep soil water allows the vegetation to dissipate heat
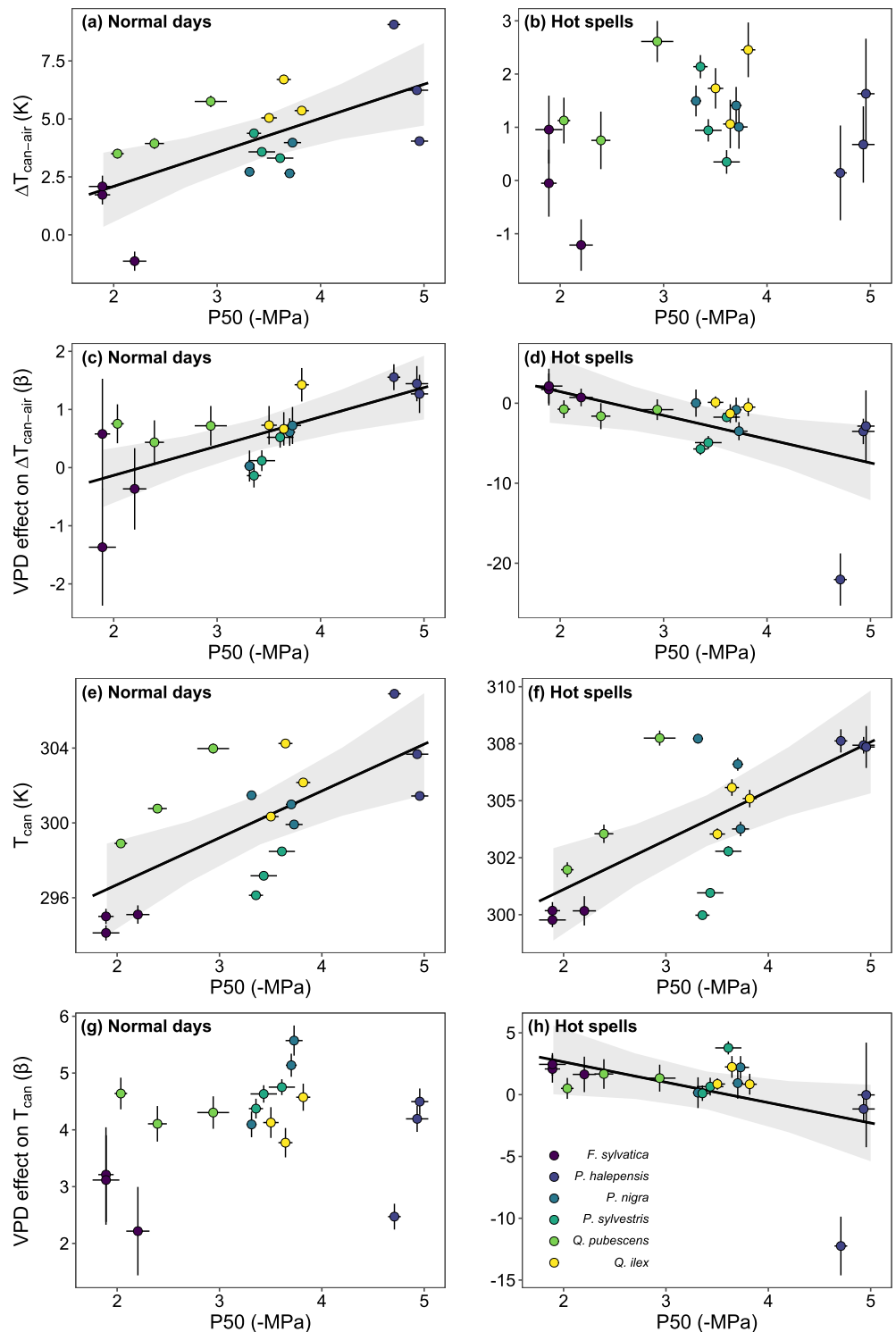
Figure 6. Correlation of the thermal balance of forests ($\Delta T_{can-air}$) and canopy temperature (T_{can}) with the xylem pressure at the 50% loss of conductivity ($P50$). Left panels (a, c, e and g) depict the linear mixed-model fits (species as random factor) between the average $\Delta T_{can-air}$ (a), the β coefficients of the vapor deficit pressure (VPD) effect on $\Delta T_{can-air}$ (b), T_{can} (c) and the β coefficients of the vapor deficit pressure (VPD) effect on T_{can}. Right panels (b, d, f and h) depict the same but for hot spells. Significant correlations are shown by solid lines and the corresponding p value is shown at the bottom right of each panel. Dashed lines represent marginally significant correlations. Fill colors show the different species included in the analysis.

through evaporation from the leaves, thus avoiding overheating, decreasing T_{can} and sensible heat fluxes (Krich et al., 2022). Under wet soils and high VPD, our model predicted that $\Delta T_{can-air}$ would become negative, that is, T_{can} could be cooler than T_{air} (Figure 5a). Yet, previous studies have shown that a negative $\Delta T_{can-air}$ in clear sky days is rare for temperate forests and that it can only be expected in systems such as rice paddies where water supply is unlimited (Still et al., 2022), or during rain events (van Dijk et al., 2015). Because our remotely sensed T_{air} is only available for clear sky days, the predicted low $\Delta T_{can-air}$ was most likely caused by the occurrence of heat advection in combination with s sufficient soil water availability to supply transpiration during hot spells, instead of by a VPD-induced transpiration increase, as indicated above.

4.3. Biotic Controls on Forest $\Delta T_{can-air}$

We found significant but quantitatively small differences in $\Delta T_{can-air}$ among forests dominated by species belonging to different functional groups (Figure 3a). For example, the thermal balance of needleleaf montane forests did not differ from that of broadleaf deciduous, despite their slightly different climatic niches (Table S1 in Supporting Information S1). $\Delta T_{can-air}$ differed among forests dominated by functional groups occupying contrasting climatic niches (see summer PPET in Table S1 in Supporting Information S1), but also presenting substantial structural differences (Table S2 in Supporting Information S1). For example, we found that $\Delta T_{can-air}$ was higher in broadleaf evergreen forests than in the also drought-adapted needleleaf Mediterranean (Table S1 in Supporting Information S1 and Figure 3b). Still, $\Delta T_{can-air}$ in broadleaf evergreen forests was not statistically different to the structurally and climatically different needleleaf montane forests. The differences in T_{can} between functional groups are constrained by the background climatic conditions (i.e., gradients in MAT), but for $\Delta T_{can-air}$ the differences among groups were possibly modified by contrasting surface properties and forest functioning. This was further confirmed by the analysis of the drivers of $\Delta T_{can-air}$ showing significant effects of MAP and MAT, but also of forest structural variables such as albedo, mean tree height or tree cover (Figure 4). The discrete nature of functional groups may be too limiting to describe continuous fluxes such as those involved in the forest thermal balance (Bodegom et al., 2012). Indeed, the intra-group variability in $\Delta T_{can-air}$ was high within all groups (Figure 3), in agreement with previous studies suggesting that site-specific conditions may be more relevant than plant functional groups (Wang et al., 2019) or leaf-level traits (Blonder et al., 2020) for the surface energy balance.

The structure of forests appeared almost as determinant as daily meteorological conditions for $\Delta T_{can-air}$. In contrast, T_{can} mostly varied as a function of daily VPD and CWB (Figure 4). As hypothesized, we found significant correlations of forest structural variables that determine heat dissipation mechanisms. The model showed that tall and dense forests with a canopy fully covering the ground maintained a cooler T_{can} relative to T_{air}, compared to forests with short trees with sparse stems and canopies. Albedo affected positively both $\Delta T_{can-air}$ and T_{can}. This positive effect on $\Delta T_{can-air}$ or T_{can} may be the consequence of the higher albedos of forests adapted to warmer temperatures and with a more conservative water use (Muller et al., 2021). Albedo is indeed lower in montane needleleaf forests, compared to Mediterranean needleleaf ones (Table S2 in Supporting Information S1). Similarly, $\Delta T_{can-air}$ is higher in those stands occupying drier areas and composed by species with functional traits associated with a more efficient water use and a higher resistance to drought (Table S3 in Supporting Information S1 and Figure 6a), as expected. In addition, the response of $\Delta T_{can-air}$ to VPD is clearly positive in drier stands (Figure 6c). Interestingly, this relationship was reversed during hot spells (Table S3 in Supporting Information S1 and Figure 6d). During hot spells, the $\Delta T_{can-air}$ did not respond to VPD in drought-sensitive species such as *F. sylvatica* (Figure 6d). In contrast, $\Delta T_{can-air}$ and T_{can} were disproportionately reduced by VPD during hot spells in drought-resistant conifer species, such as *P. halepensis* (Sánchez-Costa et al., 2015). This trait-mediated disparity in species-specific (and intra-specific) response to VPD during hot spells is in agreement with the observations of high transpiration during extremely high VPD conditions in Australian Mediterranean woodlands (Krich et al., 2022), but only for certain ecosystems with access to groundwater. The capacity to tap on deep water sources in Mediterranean ecosystem may be key to sustain transpiration under high VPD and heat stress.

5. Conclusions

Here we used a novel approach combining high-resolution remotely sensed land surface temperature with a suite of ground-based structural and functional forest data to investigate the environmental determinants of the forest

thermal balance for a Mediterranean region. We found that the forest thermal balance during hot spells was more dependent on heat advection episodes suddenly increasing T_{air} than on T_{can}. This pattern is fundamentally different to the strong influence of surface responses in less water-limited regions (Lansu et al., 2020; Teuling et al., 2010; Wang et al., 2019). In fact, background climatic conditions explained a significant part of the variability in $\Delta T_{can-air}$ in our study area, which also contains relatively moist forests analogous to those in temperate regions, as central Europe. Furthermore, we found that climatic water availability and the plant water use strategy exert additional controls on the forest thermal balance, probably through transpiration cooling. The coordination of rooting depth and other plant functional traits linked to water-use strategies (Illuminati et al., 2022) may underlie the association of the considered traits with the response to increased VPD during hot spells, that included canopy cooling in the driest stands of the most drought-resistant species (Figure 6h). Finally, we also showed that forest structural characteristics related to surface roughness such as tree height and cover, stand density, and albedo also influence the forest thermal balance, as they affect heat dissipation mechanisms (Muller et al., 2021). Therefore, our results demonstrate that the integration of functional traits and forest structure over relevant spatial scales could improve our ability to understand and model land–atmosphere feedbacks in forested regions.

Conflict of Interest

The authors declare no conflicts of interest relevant to this study.

Data Availability Statement

The data that support the findings of this study are openly available in the Zenodo repository at https://zenodo.org/record/7254572, full details are given in the next section (Barbeta et al., 2022).

References

Akaike, H. (1974). A new look at the statistical model identification. *IEEE Transactions on Automatic Control*, *19*(6), 716–723. https://doi.org/10.1109/TAC.1974.1100705

Anderegg, W. R. L., Konings, A. G., Trugman, A. T., Yu, K., Bowling, D. R., Gabbitas, R., et al. (2018). Hydraulic diversity of forests regulates ecosystem resilience during drought. *Nature*, *561*(7724), 538–541. https://doi.org/10.1038/s41586-018-0539-7

Anderegg, W. R. L., Trugman, A. T., Bowling, D. R., Salvucci, G., & Tuttle, S. E. (2019). Plant functional traits and climate influence drought intensification and land–atmosphere feedbacks. *Proceedings of the National Academy of Sciences of the United States of America*, *116*(28), 14071–14076. https://doi.org/10.1073/pnas.1904747116

Bagley, J. E., Kueppers, L. M., Billesbach, D. P., Williams, I. N., Biraud, S. C., & Torn, M. S. (2017). The influence of land cover on surface energy partitioning and evaporative fraction regimes in the U.S. Southern Great Plains. *Journal of Geophysical Research*, *122*(11), 5793–5807. https://doi.org/10.1002/2017JD026740

Barbeta, A., Miralles, D. G., Mendiola, L., Gimeno, T. E., Sabaté, S., & Carnicer, J. (2022). Thermal balance of forests in the Mediterranean-temperate ecotone. https://doi.org/10.5281/ZENODO.7254572

Barbeta, A., & Peñuelas, J. (2017). Relative contribution of groundwater to plant transpiration estimated with stable isotopes. *Scientific Reports*, *7*(1), 1–10. https://doi.org/10.1038/s41598-017-09643-x

Bates, D., Mächler, M., Bolker, B. M., & Walker, S. C. (2015). Fitting linear mixed-effects models using lme4. *Journal of Statistical Software*, *67*(1), 1–48. https://doi.org/10.18637/jss.v067.i01

Beck, H. E., Zimmermann, N. E., McVicar, T. R., Vergopolan, N., Berg, A., & Wood, E. F. (2018). Present and future köppen-geiger climate classification maps at 1-km resolution. *Scientific Data*, *5*, 1–12. https://doi.org/10.1038/sdata.2018.214

Blonder, B., Escobar, S., Kapás, R. E., & Michaletz, S. T. (2020). Low predictability of energy balance traits and leaf temperature metrics in desert, montane and alpine plant communities. *Functional Ecology*, *34*(9), 1882–1897. https://doi.org/10.1111/1365-2435.13643

Bodegom, P. M. V., Douma, J. C., Witte, J. P. M., Ordoñez, J. C., Bartholomeus, R. P., Aerts, R., et al. (2012). Going beyond limitations of plant functional types when predicting global ecosystem – atmosphere fluxes: Exploring the merits of traits-based approaches (pp. 625–636). https://doi.org/10.1111/j.1466-8238.2011.00717.x

Bonan, G. (2015). *Ecological climatology: Concepts and Applications* (3rd ed.). Cambridge University Press. https://doi.org/10.1017/CBO9781107339200

Cabon, A., Martínez-Vilalta, J., Martínez, de Aragón, J., Poyatos, R., & De Cáceres, M. (2018). Applying the eco-hydrological equilibrium hypothesis to model root distribution in water-limited forests. *Ecohydrology*, *11*(7), e2015. https://doi.org/10.1002/eco.2015

Canadell, J. G., Monteiro, P. M. S., Costa, M. H., da Cunha, L., Cox, P. M., Eliseev, A. V., et al. (2021). Global carbon and other biogeochemical cycles and feedbacks. In V., Masson-Delmotte, P., Zhai, A., Pirani, S. L., Connors, C., Péan, S., Berger, et al. (Eds.), *Climate Change 2021: The Physical Science Basis. Contribution of Working Group I to the Sixth Assessment Report of the Intergovernmental Panel on Climate Change*(pp. 673–816). Cambridge University Press. https://doi.org/10.1017/9781009157896.007

Cescatti, A., Marcolla, B., Santhana Vannan, S. K., Pan, J. Y., Román, M. O., Yang, X., et al. (2012). Intercomparison of MODIS albedo retrievals and in situ measurements across the global FLUXNET network. *Remote Sensing of Environment*, *121*, 323–334. https://doi.org/10.1016/j.rse.2012.02.019

Cooley, S. S., Fisher, J. B., & Goldsmith, G. R. (2022). Convergence in water use efficiency within plant functional types across contrasting climates. *Nature Plants*, *8*(April), 341–345. https://doi.org/10.1038/s41477-022-01131-z

De Cáceres, M., Martin-StPaul, N., Turco, M., Cabon, A., & Granda, V. (2018). Estimating daily meteorological data and downscaling climate models over landscapes. *Environmental Modelling & Software*, *108*(August), 186–196. https://doi.org/10.1016/j.envsoft.2018.08.003

de Oliveira, G., Brunsell, N. A., Moraes, E. C., Shimabukuro, Y. E., dos Santos, T. V., von Randow, C., et al. (2019). Effects of land-cover changes on the partitioning of surface energy and water fluxes in Amazonia using high-resolution satellite imagery. *Ecohydrology*, *12*(6), 1–18. https://doi.org/10.1002/eco.2126

Drumond, A., Marengo, J., Ambrizzi, T., Nieto, R., Moreira, L., & Gimeno, L. (2014). The role of the Amazon basin moisture in the atmospheric branch of the hydrological cycle: A Lagrangian analysis. *Hydrology and Earth System Sciences*, *18*(7), 2577–2598. https://doi.org/10.5194/hess-18-2577-2014

Duursma, R. A., Barton, C. V. M., Lin, Y.-S., Medlyn, B. E., Eamus, D., Tissue, D. T., et al. (2014). The peaked response of transpiration rate to vapour pressure deficit in field conditions can be explained by the temperature optimum of photosynthesis. *Agricultural and Forest Meteorology*, *189*, 2–10. https://doi.org/10.1016/j.agrformet.2013.12.007

Ellison, D., Morris, C. E., Locatelli, B., Sheil, D., Cohen, J., Murdiyarso, D., et al. (2017). Trees, forests and water: Cool insights for a hot world. *Global Environmental Change*, *43*, 51–61. https://doi.org/10.1016/j.gloenvcha.2017.01.002

Fauset, S., Freitas, H. C., Galbraith, D. R., Sullivan, M. J. P., Aidar, M. P. M., Joly, C. A., et al. (2018). Differences in leaf thermoregulation and water use strategies between three co-occurring Atlantic forest tree species. *Plant, Cell and Environment*, *41*(7), 1618–1631. https://doi.org/10.1111/pce.13208

Fischer, E. M., Seneviratne, S. I., Lüthi, D., & Schär, C. (2007). Contribution of land-atmosphere coupling to recent European summer heat waves. *Geophysical Research Letters*, *34*(6), 1–6. https://doi.org/10.1029/2006GL029068

Fisher, J. B., Lee, B., Purdy, A. J., Halverson, G. H., Dohlen, M. B., Cawse-Nicholson, K., et al. (2020). ECOSTRESS: NASA's next generation mission to measure evapotranspiration from the International Space Station. *Water Resources Research*, *56*(4), 1–20. https://doi.org/10.1029/2019WR026058

Flo, V., Martinez-Vilalta, J., Granda, V., Mencuccini, M., & Poyatos, R. (2021). Vapour pressure deficit is the main driver of tree canopy conductance across biomes. *Agricultural and Forest Meteorology*, *322*, 109029. https://doi.org/10.1002/essoar.10508049.1

Forzieri, G., Alkama, R., Miralles, D. G., & Cescatti, A. (2017). Satellites reveal contrasting responses of regional climate to the widespread greening of Earth. *Science*, *1184*(June), 1180–1184. https://doi.org/10.1126/science.aal1727

Forzieri, G., Miralles, D. G., Ciais, P., Alkama, R., Ryu, Y., Duveiller, G., et al. (2020). Increased control of vegetation on global terrestrial energy fluxes. *Nature Climate Change*, *10*(4), 356–362. https://doi.org/10.1038/s41558-020-0717-0

Gerken, T., Ruddell, B. L., Yu, R., Stoy, P. C., & Drewry, D. T. (2019). Robust observations of land-to-atmosphere feedbacks using the information flows of FLUXNET. *Npj Climate and Atmospheric Science*, *2*(1), 37. https://doi.org/10.1038/s41612-019-0094-4

Grace, J. (1988). Plant response to wind. *Agriculture, Ecosystems & Environment*, *22/23*, 71–88. Elsevier Science Publishers B.V.

Green, J. K., Ballantyne, A., Abramoff, R., Gentine, P., Makowski, D., & Ciais, P. (2022). Surface temperatures reveal the patterns of vegetation water stress and their environmental drivers across the tropical Americas. *Global Change Biology*, *28*(9), 2940–2955. https://doi.org/10.1111/gcb.16139

Grossiord, C., Buckley, T. N., Cernusak, L. A., Novick, K. A., Poulter, B., Siegwolf, R. T. W., et al. (2020). Plant responses to rising vapor pressure deficit. *New Phytologist*, *226*(6), 1550–1566. https://doi.org/10.1111/nph.16485

Hulley, G. C., Göttsche, F. M., Rivera, G., Hook, S. J., Freepartner, R. J., Martin, M. A., et al. (2022). Validation and quality assessment of the ECOSTRESS level-2 land surface temperature and emissivity product. *IEEE Transactions on Geoscience and Remote Sensing*, *60*, 1–23. https://doi.org/10.1109/TGRS.2021.3079879

Illuminati, A., Querejeta, J. I., Pías, B., Escudero, A., & Matesanz, S. (2022). Coordination between water uptake depth and the leaf economic spectrum in a Mediterranean shrubland. *Journal of Ecology*, *110*(January), 1–13. https://doi.org/10.1111/1365-2745.13909

IPCC. (2021). *Climate Change 2021: The Physical Science Basis. Contribution of Working Group I to the Sixth Assessment Report of the Intergovernmental Panel on Climate Change*. Cambridge University Press. https://doi.org/10.1017/9781009157896

Javadian, M., Smith, W. K., Lee, K., Knowles, J. F., Scott, R. L., Fisher, J. B., et al. (2022). Canopy temperature is regulated by ecosystem structural traits and captures the ecohydrologic dynamics of a semiarid mixed conifer forest site. *Journal of Geophysical Research: Biogeosciences*, *127*(2), 1–15. https://doi.org/10.1029/2021JG006617

Keune, J., & Miralles, D. G. (2019). A precipitation recycling network to assess freshwater vulnerability: Challenging the watershed convention. *Water Resources Research*, *55*(11), 9947–9961. https://doi.org/10.1029/2019wr025310

Knauer, J., El-Madany, T. S., Zaehle, S., & Migliavacca, M. (2018). Bigleaf—An R package for the calculation of physical and physiological ecosystem properties from eddy covariance data. *PLoS One*, *13*(8), 1–26. https://doi.org/10.1371/journal.pone.0201114

Koster, R. D., Dirmeyer, P. A., Guo, Z., Bonan, G., Chan, E., Cox, P., et al. (2004). Regions of strong coupling between soil moisture and precipitation. *Science*, *305*(5687), 1138–1140. https://doi.org/10.1126/science.1100217

Krich, C., Mahecha, M. D., Migliavacca, M., De Kauwe, M. G., Griebel, A., Runge, J., & Miralles, D. G. (2022). Decoupling between ecosystem photosynthesis and transpiration: A last resort against overheating. *Environmental Research Letters*, *17*(4), 44013. https://doi.org/10.1088/1748-9326/ac583e

Lansu, E. M., van Heerwaarden, C. C., Stegehuis, A. I., & Teuling, A. J. (2020). Atmospheric aridity and apparent soil moisture drought in European forest during heat waves. *Geophysical Research Letters*, *47*(6). https://doi.org/10.1029/2020GL087091

Lenth, R., Singmann, H., Love, J., Buerkner, P., & Herve, M. (2018). Emmeans: Estimated marginal means, aka least-squares means (Vol. *1*(1), p. 3). R Package Version.

Llebot, J. E. (2005). Informe sobre el canvi climàtic a Catalunya.

Lüdecke, D., Makowski, D., Waggoner, P., & Patil, I. (2020). *Package "performance": Assessment of regression models performance*. CRAN.R.

Mac Nally, R., & Walsh, C. J. (2004). Hierarchical partitioning public-domain software. *Biodiversity & Conservation*, *13*(3), 659–660. https://doi.org/10.1023/B:BIOC.0000009515.11717.0b

Martín Vide, J. (2016). *Tercer Informe sobre el canvi climàtic de Catalunya*. Insitut d'Estudis Catalans i Generalitat de Catalunya.

Massmann, A., Gentine, P., & Lin, C. (2019). When does vapor pressure deficit drive or reduce evapotranspiration? *Journal of Advances in Modeling Earth Systems*, *11*(10), 3305–3320. https://doi.org/10.1029/2019MS001790

Meier, R., Davin, E. L., Swenson, S. C., Lawrence, D. M., & Schwaab, J. (2019). Biomass heat storage dampens diurnal temperature variations in forests. *Environmental Research Letters*, *14*(8), 084026. https://doi.org/10.1088/1748-9326/ab2b4e

Migliavacca, M., Musavi, T., Mahecha, M. D., Nelson, J. A., Knauer, J., Baldocchi, D. D., et al. (2021). The three major axes of terrestrial ecosystem function. *Nature*, *598*(7881), 468–472. https://doi.org/10.1038/s41586-021-03939-9

Miralles, D. G., Gentine, P., Seneviratne, S. I., & Teuling, A. J. (2019). Land–atmospheric feedbacks during droughts and heatwaves: State of the science and current challenges. *Annals of the New York Academy of Sciences*, *1436*(1), 19–35. https://doi.org/10.1111/nyas.13912

Miralles, D. G., Teuling, A. J., Van Heerwaarden, C. C., & De Arellano, J. V. G. (2014). Mega-heatwave temperatures due to combined soil desiccation and atmospheric heat accumulation. *Nature Geoscience*, *7*(5), 345–349. https://doi.org/10.1038/ngeo2141

Moyano, M. C., Garcia, M., Palacios-Orueta, A., Tornos, L., Fisher, J. B., Fernández, N., et al. (2018). Vegetation water use based on a thermal and optical remote sensing model in the Mediterranean Region of Doñana. *Remote Sensing*, *10*(7), 1105. https://doi.org/10.3390/rs10071105

Muller, J. D., Rotenberg, E., Tatarinov, F., Oz, I., & Yakir, D. (2021). Evidence for efficient nonevaporative leaf-to-air heat dissipation in a pine forest under drought conditions. *New Phytologist*, *232*(6), 2254–2266. https://doi.org/10.1111/nph.17742

Murray, K., & Conner, M. M. (2009). Methods to quantify variable importance: Implications for the analysis of noisy ecological data. *Ecology*, *90*(2), 348–355. https://doi.org/10.1890/0012-9658-90.5.1425

Nemani, R. R., Running, S. W., Pielke, R. A., & Chase, T. N. (1996). Global vegetation cover changes from coarse resolution satellite data. *Journal of Geophysical Research*, *101*(D3), 7157–7162. https://doi.org/10.1029/95JD02138

O'Connor, J. C., Dekker, S. C., Staal, A., Tuinenburg, O. A., Rebel, K. T., & Santos, M. J. (2021). Forests buffer against variations in precipitation. *Global Change Biology*, *27*(19), 4686–4696. https://doi.org/10.1111/gcb.15763

Pitman, A. J. (2003). The evolution of, and revolution in, land surface schemes designed for climate models. *International Journal of Climatology*, *23*(5), 479–510. https://doi.org/10.1002/joc.893

R Core Team. (2021). *R: A language and environment for statistical computing*. R Foundation for Statistical Computing.

Roces-díaz, J. V., Vayreda, J., Banqué-casanovas, M., Cusó, M., Anton, M., Bonet, J. A., et al. (2018). Assessing the distribution of forest ecosystem services in a highly populated Mediterranean region. *Ecological Indicators*, *93*(October 2016), 986–997. https://doi.org/10.1016/j.ecolind.2018.05.076

Rosas, T., Mencuccini, M., Barba, J., Cochard, H., Saura-Mas, S., & Martínez-Vilalta, J. (2019). Adjustments and coordination of hydraulic, leaf and stem traits along a water availability gradient. *New Phytologist*, *223*(2), 632–646. https://doi.org/10.1111/nph.15684

Sánchez-Costa, E., Poyatos, R., & Sabaté, S. (2015). Contrasting growth and water use strategies in four co-occurring Mediterranean tree species revealed by concurrent measurements of sap flow and stem diameter variations. *Agricultural and Forest Meteorology*, *207*, 24–37. https://doi.org/10.1016/j.agrformet.2015.03.012

Schumacher, D. L., Keune, J., van Heerwaarden, C. C., de Vilà-Guerau Arellano, J., Teuling, A. J., & Miralles, D. G. (2019). Amplification of mega-heatwaves through heat torrents fuelled by upwind drought. *Nature Geoscience*, *12*(9), 712–717. https://doi.org/10.1038/s41561-019-0431-6

Seneviratne, S. I., Zhang, X., Adnan, M., Badi, W., Dereczynski, C., Di Luca, A., et al. (2021). Weather and climate extreme events in a changing climate. In V., Masson-Delmotte, P., Zhai, A., Pirani, S. L., Connors, C., Péan, S., Berger, et al. (Eds.), *Climate Change 2021: The Physical Science Basis. Contribution of Working Group I to the Sixth Assessment Report of the Intergovernmental Panel on Climate Change* (pp. 1513–1766). Cambridge University Press. https://doi.org/10.1017/9781009157896.013

Shiflett, S. A., Liang, L. L., Crum, S. M., Feyisa, G. L., Wang, J., & Jenerette, G. D. (2017). Variation in the urban vegetation, surface temperature, air temperature nexus. *Science of the Total Environment*, *579*, 495–505. https://doi.org/10.1016/j.scitotenv.2016.11.069

Sousa, P. M., Barriopedro, D., Ramos, A. M., García-Herrera, R., Espírito-Santo, F., & Trigo, R. M. (2019). Saharan air intrusions as a relevant mechanism for Iberian heatwaves: The record breaking events of August 2018 and June 2019. *Weather and Climate Extremes*, *26*, 100224. https://doi.org/10.1016/j.wace.2019.100224

Still, C. J., Page, G., Rastogi, B., Griffith, D. M., Aubrecht, D. M., Kim, Y., et al. (2022). No evidence of canopy-scale leaf thermoregulation to cool leaves below air temperature across a range of forest ecosystems. *Proceedings of the National Academy of Sciences*, *119*(38), e2205682119. https://doi.org/10.1073/pnas.2205682119

Still, C. J., Rastogi, B., Page, G. F. M., Griffith, D. M., Sibley, A., Schulze, M., et al. (2021). Imaging canopy temperature: Shedding (thermal) light on ecosystem processes. *New Phytologist*, *230*(5), 1746–1753. https://doi.org/10.1111/nph.17321

te Wierik, S. A., Cammeraat, E. L. H., Gupta, J., & Artzy-Randrup, Y. A. (2021). Reviewing the Impact of Land Use and Land-Use Change on Moisture Recycling and Precipitation Patterns. *Water Resources Research*, *57*(7). https://doi.org/10.1029/2020WR029234

Teuling, A. J., Seneviratne, S. I., Stöckli, R., Reichstein, M., Moors, E., Ciais, P., et al. (2010). Contrasting response of European forest and grassland energy exchange to heatwaves. *Nature Geoscience*, *3*(10), 722–727. https://doi.org/10.1038/ngeo950

van Dijk, A. I. J. M., Gash, J. H., van Gorsel, E., Blanken, P. D., Cescatti, A., Emmel, C., et al. (2015). Rainfall interception and the coupled surface water and energy balance. *Agricultural and Forest Meteorology*, *214–215*, 402–415. https://doi.org/10.1016/j.agrformet.2015.09.006

Wang, P., Li, D., Liao, W., Rigden, A., & Wang, W. (2019). Contrasting evaporative responses of ecosystems to heatwaves traced to the opposing roles of vapor pressure deficit and surface resistance. *Water Resources Research*, *55*(6), 4550–4563. https://doi.org/10.1029/2019WR024771

Williams, I. N., & Torn, M. S. (2015). Vegetation controls on surface heat flux partitioning, and land-atmosphere coupling. *Geophysical Research Letters*, *42*(21), 9416–9424. https://doi.org/10.1002/2015GL066305

Xiao, J., Fisher, J. B., Hashimoto, H., Ichii, K., & Parazoo, N. C. (2021). Emerging satellite observations for diurnal cycling of ecosystem processes. *Nature Plants*, *7*(7), 877–887. https://doi.org/10.1038/s41477-021-00952-8

Yan, J. W., Liu, J. Y., Chen, B. Z., Feng, M., Fang, S. F., Xu, G., et al. (2014). Changes in the land surface energy budget in eastern China over the past three decades: Contributions of land-cover change and climate change. *Journal of Climate*, *27*(24), 9233–9252. https://doi.org/10.1175/JCLI-D-13-00492.1

Yi, K., Smith, J. W., Jablonski, A. D., Tatham, E. A., Scanlon, T. M., Lerdau, M. T., et al. (2020). High heterogeneity in canopy temperature among Co-occurring tree species in a temperate forest. *Journal of Geophysical Research: Biogeosciences*, *125*(12). https://doi.org/10.1029/2020JG005892

Zhang, Q., Barnes, M., Benson, M., Burakowski, E., Oishi, A. C., Ouimette, A., et al. (2020). Reforestation and surface cooling in temperate zones: Mechanisms and implications. *Global Change Biology*, *26*(6), 3384–3401. https://doi.org/10.1111/gcb.15069

Zhu, Z., Piao, S., Myneni, R. B., Huang, M., Zeng, Z., Canadell, J. G., et al. (2016). Greening of the Earth and its drivers. *Nature Climate Change*, *6*(8), 791–795. https://doi.org/10.1038/nclimate3004